DOI: 10.1002/ejic.200701368

Nanostructured Titania–Diphosphonate Hybrid Materials with a Porous Hierarchy

Xue-Jun Zhang,[a][‡] Tian-Yi Ma,[a][‡] and Zhong-Yong Yuan*[a]

Keywords: Nanostructure / Titanium phosphonates / Hierarchical porosity / Organic–inorganic hybrids / Self-assembly

An organic–inorganic hybrid nanostructured material of titania–diphosphonate (Ti-HEDP) was prepared from a simple self-assembly process with the precursor tetrabutyl titanate and 1-hydroxyethane-1,1-diphosphonic acid (HEDP). The prepared hybrid Ti-HEDP has a semicrystalline anatase phase, exhibiting a hierarchical macroporous structure composed of mesostructured Ti-HEDP nanorods with a length of 80–150 nm and a thickness of 18–38 nm. The BET surface area is 257 m^2/g. The 1-hydroxyethane-1,1-diyl-bridged organophosphonate groups were homogeneously incorported into the network of the hierarchical nanostructured/porous solid, as revealed by FT-IR spectroscopy, MAS NMR spectroscopy, XPS, and TGA measurements. The optical property, photocatalytic activity, and metal ion adsorption ability of the hierarchical Ti-HEDP materials were also investigated, suggesting that they have potential applications in catalysis and adsorption.

Introduction

Recent works have been aimed at the rational synthesis of organically functionalized porous metal phosphonate and metal oxide/organophosphonate hybrid materials[1–5] because of their multifunctionality, from both the inorganic and organic components, and hence their potential in the fields of optics, electronics, membranes, catalysis, adsorption, etc. Some of the alkylmonophosphonic acids and their derivatives (salts, esters) have been used as organophosphorus coupling molecules to modify metal-oxide surfaces by grafting.[6,7] Alternatively a two-step nonhydrolytic/hydrolytic sol-gel process was performed to prepare metal oxide/organophosphonate hybrids, in which the organophosphorus coupling molecules were incorporated into the inorganic network.[8] Several mesoporous aluminum organophosphonate materials were also reported recently, obtained from a surfactant-templating method,[5,9] and macroporous titanium-phosphonate hybrids were prepared with the use of polystyrene spheres as a template.[10] However, little research deals with the nanostructure and hierarchical porosity of the metal and oxide phosphonate hybrids, even though their multifunctionality may benefit from the hierarchical porous nanostructure. Song et al. synthesized metal phenylphosphonate nanoparticles and nanorods by surfactant-assisted methods.[11,12] Vasylyev et al. reported titanium and oxide–phosphonate porous nanospherical particles by nonhydrolytic condensation of water-insoluble arylphosphoric acid [tetrakis-1,3,5,7-(4-phosphonatophenyl)adamantane] and titanium isopropoxide.[13] The assembly of individual nanostructured particles of metal organophosphonate into hierarchical nanoarchitectures with complex shapes for multifunctionalization and their potential applications is still a challenge. In this work, we report on the preparation of nanostructured titania–diphosphonate material with a porous hierarchy, in which hydroxyethylidene groups were anchored in the titania–phosphonate network. Mesostructured titania–diphosphonate nanorods assembled spontaneously into a hierarchically macroporous nanoarchitecture, exhibiting an efficient photocatalytic performance and heavy metal ion adsorption behavior.

Results and Discussion

The XRD pattern of the synthesized Ti-HEDP presents several very weak diffraction peaks, which could be identified as an anatase phase, while pure titania obtained in the absence of phosphonic acid shows the bicrystalline phases of anatase and brookite (Figure 1). This indicates that the hydrolysis of titanium alkoxide in the phosphonic acid solution resulted in the incorporation of organophosphonate into the titania network, leading to semicrystalline anatase nanoparticles of about 3 nm in size linked to each other by amorphous titanium-phosphonate nanoclusters. Figure 2 shows the SEM and TEM images of the synthesized Ti-HEDP. A large number of alveolate macropores with openings ranging from 90 to 400 nm spread over the

[a] Institute of New Catalytic Materials Science, Engineering Research Center of Energy Storage and Conversion (Ministry of Education), College of Chemistry, Nankai University, Tianjin 300071, China
Fax: +86-22-23509610
E-mail: zyyuan@nankai.edu.cn
[‡] These authors have made an equal contribution to this work.

entire structure, among which several huge macrochannels with diameters in the micrometer scale (mainly 1–3 μm) are interspersed. The macroporous frameworks are composed of uniform nanorods of 80–150 nm in length and 18–38 nm in thickness, and "worm-eaten" disordered mesostructures are also observed in these nanorods.

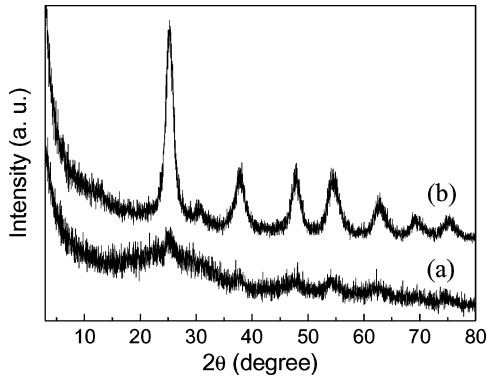

Figure 1. XRD patterns of the synthesized (a) Ti-HEDP and (b) pure titania.

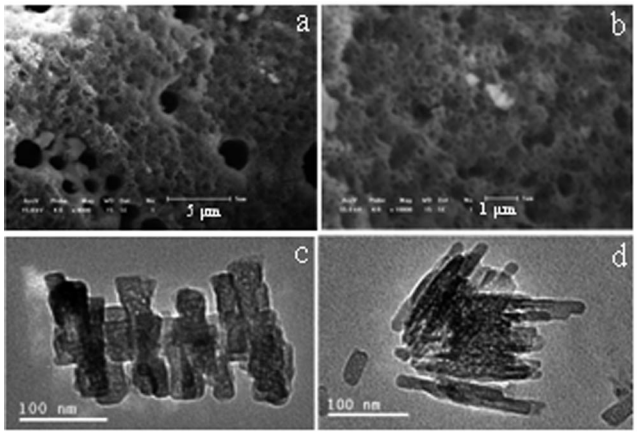

Figure 2. SEM (a,b) and TEM (c,d) images of the synthesized Ti-HEDP.

The hydrolysis of tetrabutyl titanate precursors in organophosphonic acid solution results in the rapid formation of nanometer-sized titanium phosphonate sols, titanium oxo clusters, as well as nanosized phosphonated titania particles, where Ti–O–P bridges are easily obtained from the reaction Ti–OBu + P–OH → Ti–O–P + BuOH. Meanwhile, a lot of butanol molecules are generated and give a multiple component system of alkoxide/organophosphonate alcohol (butanol, ethanol)/water, and thus microemulsion drops are formed under mild stirring. The interfacial microemulsion polymerization of titanium phosphonate sols and titanium oxo clusters rendered the formation of mesostructured titania–phosphonate nanorods with homogenously attached organophosphonate units,[14] which further aggregated along with the microemulsions to give a hierarchical macroporous structure (Figure 3). In this process, phase separation might take place in the growing aggregates of Ti-HEDP-based mesophases and water/alcohol domains,[15,16] leading to the creation of huge, sporadic macrochannels in hierarchical macroporous networks.

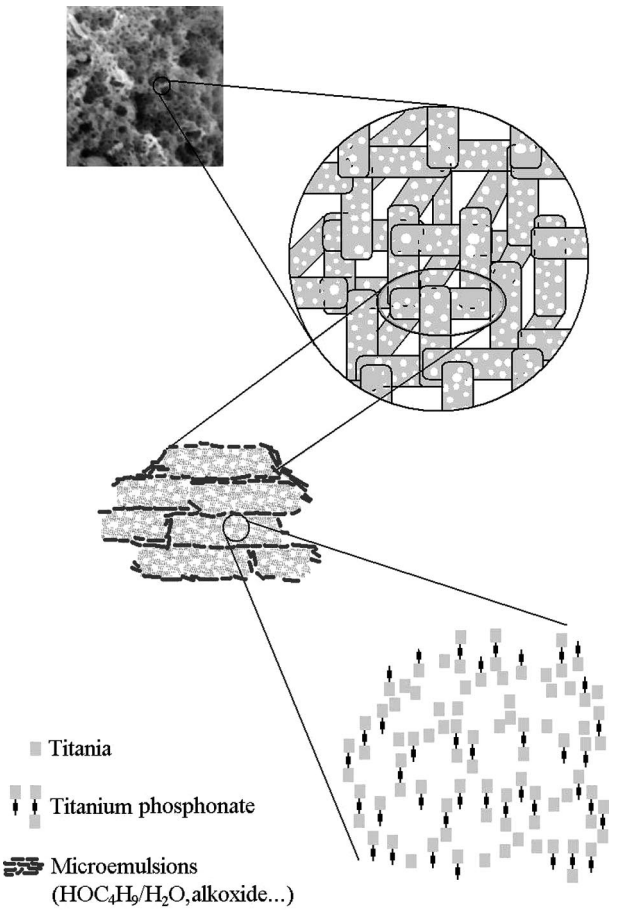

Figure 3. Schematic structure and proposed mechanism of Ti-HEDP.

Figure 4 shows the N_2 adsorption–desorption isotherms and the corresponding pore size distribution curves of the hybrid Ti-HEDP and pure titania. The isotherm of Ti-HEDP is of type II, showing a gradual increase of nitrogen-adsorbed volume with an increase in the relative pressure, which has been observed previously in several as-synthesized surfactant-containing mesoporous silica materials,[17,18] and some macroporous materials.[19] The adsorption and desorption branches of the isotherm do not coincide, which is because of the existence of the organic species and the effect of pore connectivity. The pore size distribution curve derived from the adsorption branch of the isotherm using the BJH method exhibits an asymmetric peak maximized at 2.0 nm, which corresponds to the irregular mesostructure observed in titania–phosphonate hybrid nanorods (Figure 2). The multi-point BET surface area is 257 m^2/g with a total pore volume of 0.263 cm^3/g. While the isotherm of pure titania is of type IV with a type H2 hysteresis loop, and its pore size distribution is centered at 2.2 nm with a BET surface area of 245 m^2/g and a total pore volume of 0.265 cm^3/g. This suggests that the synthesized Ti-HEDP and pure titania have similar textural properties.

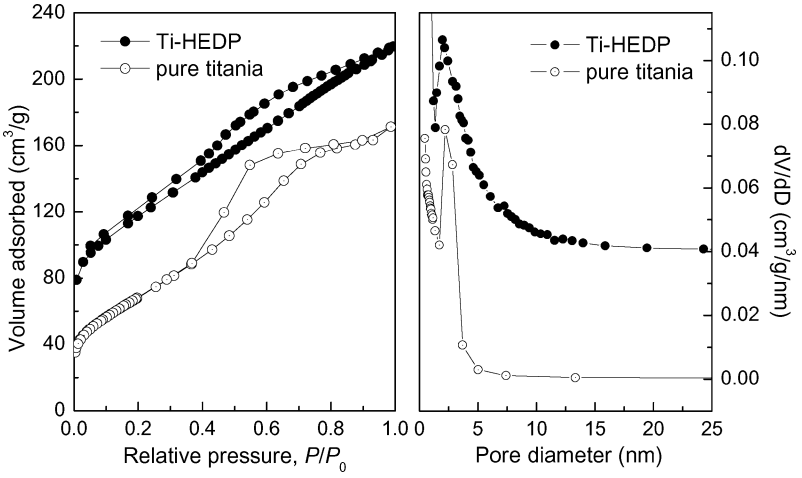

Figure 4. N_2 adsorption–desorption isotherms (left) and the BJH adsorption pore size distribution curves (right) of the Ti-HEDP sample and pure titania. The volume adsorbed and the dV/dD value were shifted +50 and +0.04 for Ti-HEDP, respectively.

The FT-IR spectrum of Ti-HEDP is shown in Figure 5, and is compared with the spectrum of HEDP. The broad band at 3400 cm^{-1} and the sharp band at 1638 cm^{-1} correspond to the surface-adsorbed water and hydroxyl groups. The strong band at 1046–1150 cm^{-1} is from the phosphonate P–O···Ti stretching vibrations. An obvious absorption peak at 928 cm^{-1} assigned to P–O···H is observed in the infrared spectrum of HEDP but absent for Ti-HEDP,[8a,13] suggesting the extensive condensation between Ti–OBu and P–OH groups to form Ti–O–P bridges. The bands at 1380 and 1450 cm^{-1}, attributed to C–O and P–C stretching vibrations, respectively,[7,20] still remain in Ti-HEDP. This implies that the organophosphonate groups retain their integrity in Ti-HEDP.

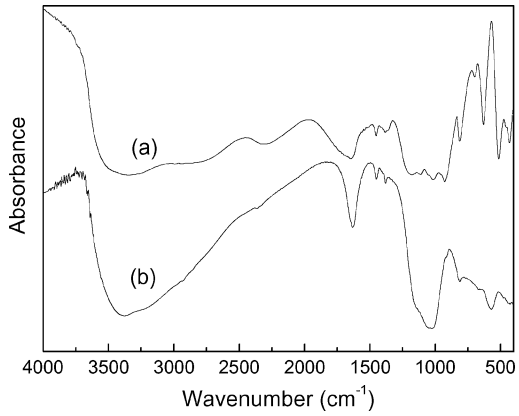

Figure 5. FT-IR spectra of (a) HEDP and (b) Ti-HEDP.

The ^{31}P MAS NMR spectrum of the resultant Ti-HEDP sample shows the resonance at δ = 16 ppm (Figure 6), which can be attributed to diphosphonate groups [≡P–C-(OH)(CH_3)–P≡] linked to the Ti atoms.[5,10] The sharp ^{31}P NMR resonance signal for layered titanium phosphonate was not observed at δ = –4 ppm.[8a,21] A ^{13}C MAS NMR spectrum of the sample exhibits resonances at δ = 20 and 69 ppm (Figure 6), which correspond to the C atoms of the terminal CH_3 group and the quaternary carbon atom connected with the P=O group of the phosphonate, respectively. It is thus deduced from the FT-IR and NMR spectroscopic results that organophosphonate groups are homogeneously anchored in the hierarchical nanostructured/porous solid.

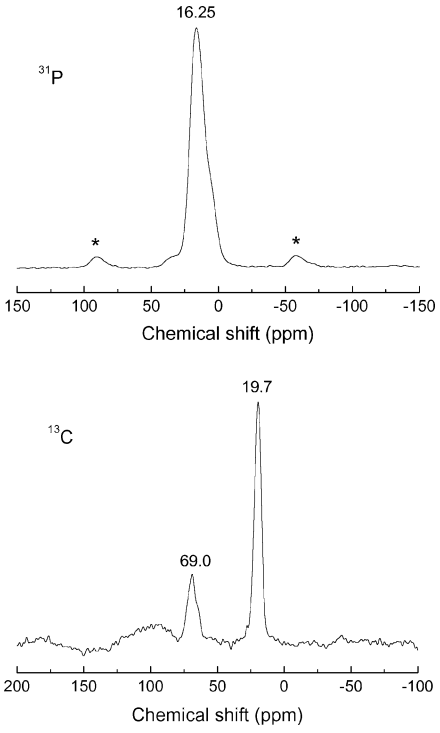

Figure 6. ^{31}P and ^{13}C MAS NMR spectra of Ti-HEDP.

High-resolution XPS spectra were also taken on the surface of the Ti-HEDP sample for an investigation of the chemical state and surface stoichiometry (Figure 7). The Ti 2p line of the Ti-HEDP sample is composed of two single peaks situated at 459.4 eV for Ti 2p3/2 and 465.2 eV for Ti 2p1/2, which are characteristic of Ti^{4+}. The P 2p binding energy of Ti-HEDP is observed around 133.1 eV, characteristic of P^{5+} in phosphonate groups. No peaks of Ti–P bonds

appear at 128.6 eV. The broad O 1s signal might be fitted by four components, situated at 530.7, 531.4, 532.1, and 533.0 eV, ascribed to the oxygen contribution from the Ti–O, P–O, O–H, and C–O bonds, respectively.[16a] The surface atomic composition was calculated as 4.31% for Ti, 10.58% for P, 38.76% for C, and 44.58% for O. The Ti/P ratio is almost 1:2, and a molecular unit of $[Ti\{O_3PC(CH_3)(OH)PO_3\}]\cdot xH_2O$ can be formulated for Ti-HEDP. Alternative formulation can be expressed as $[Ti(HEDP)]\cdot xH_2O$, which is mostly consistent with the data from the elemental microanalysis (experimental 15.55% Ti, 12.31% P, 6.03% C, and 5.29% H by mass), suggesting compositional homogeneity throughout the hybrid material. As for pure titania, the chemical analysis revealed 57.32% of Ti and 0.47% of H, but no P and N were detected, revealing pure $TiO_2\cdot xH_2O$.

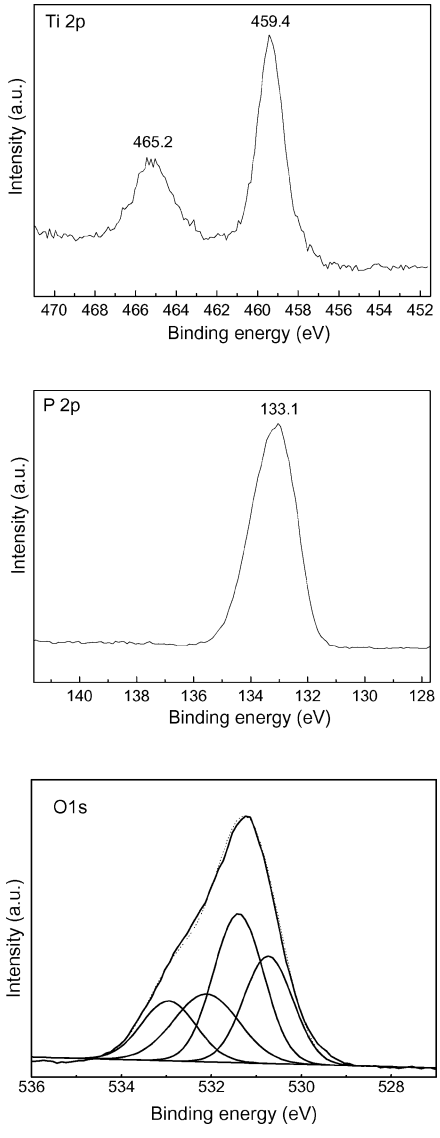

Figure 7. High-resolution XPS spectra of the Ti 2p, P 2p, and O 1s regions of Ti-HEDP.

The amount of water and the thermal stability of Ti-HEDP were determined by thermal gravimetric analysis (TGA) and differential scanning calorimetry (DSC). The TGA curve shown in Figure 8 demonstrates an initial weight loss of 10.77% from room temperature to 217 °C, accompanied by an endothermal peak around 108 °C in the DSC curve, which may be assigned to the desorption of the adsorbed and intercalated water. The weight loss of 7.24% from 217 to 620 °C, accompanied by two exothermic peaks at 308 and 556 °C, can be attributed to the decomposition of the organic species and the coke combustion. Thus, 1.7 molecules H_2O per formula unit were calculated.

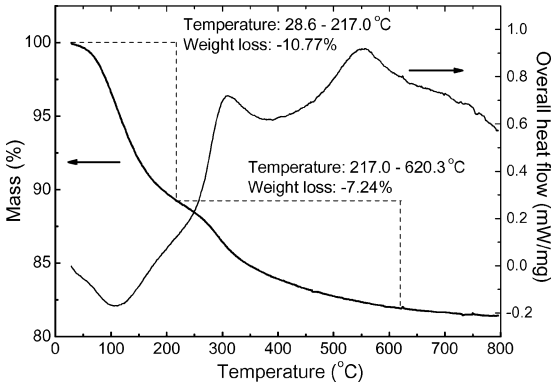

Figure 8. TGA and DSC curves for Ti-HEDP.

UV/Vis diffuse reflectance spectroscopy was performed to assess the optical properties and electronic structure of the hierarchical Ti-HEDP. Figure 9 presents the diffuse reflectance spectra of the Ti-HEDP and pure TiO_2 samples, where a low reflectance means a high absorption in the corresponding wavelength. The onset wavelength of absorption (λ_{onset}) for Ti-HEDP is about 423 nm, which is larger than that of pure TiO_2 (about 400 nm). The bandgap value (E_g) of the Ti-HEDP is estimated to be 2.93 eV from absorption spectra by a linear fit of the square root of the absorption coefficient ($\alpha_{1/2}$) as a function of the photon energy ($h\nu$) near the bandgap.[22] Compared with the E_g of pure TiO_2 (3.10 eV), the bandgap narrowing observed in Ti-HEDP should be the result of the homogeneous doping of phosphorus into the framework of the hierarchically nanostructured titania–phosphonate material.

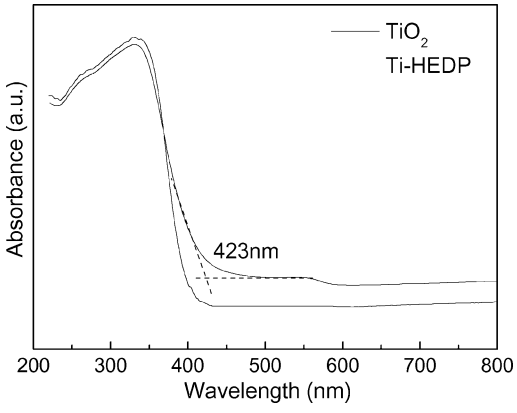

Figure 9. UV/Vis. Diffuse reflectance spectra of Ti-HEDP and pure TiO_2.

The photocatalytic activities of the synthesized hierarchical nanostructured titania–phosphonate materials were evaluated by photodegradation of Rhodamine B (RhB) under UV and visible-light irradiation (Figure 10), and compared with that of the pure TiO_2. A blank experiment (self-photosensitized process) was also performed in the absence of any catalysts for comparison. As shown in Figure 8, Ti-HEDP exhibited higher photocatalytic activity than the pure TiO_2, whether under UV or visible-light irradiation. The photocatalytic degradation rate constants (k) of Ti-HEDP and pure TiO_2, calculated by a pseudo-first-order expression, are 0.01677 and 0.01479 when under UV irradiation, while 0.00556 and 0.0037 under visible-light irradiation. Because of the similar surface areas of the synthesized Ti-HEDP (257 m^2/g) and pure titania (245 m^2/g), the influence of the surface area on the photocatalytic ability can be ignored. The efficient photocatalytic ability of the hierarchical nanostructured titania–phosphonate material should be a result of the homogeneous incorporation of phosphonate groups into the titania framework.

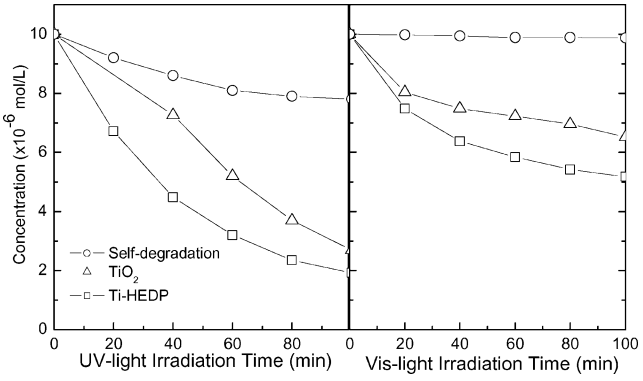

Figure 10. Photocatalytic activities of Ti-HEDP for RhB degradation under (left) UV and (right) visible-light irradiation.

The potential of the hybrid material to remove the heavy metal ions was tested in batch mode by treating 50 mL of 10, 20, and 30 mg/L of homoionic nitrate solutions of Cd^{II}, Cu^{II}, and Pb^{II} with 10 mg of the hierarchical Ti-HEDP adsorbents for 3 h. UV/Vis spectroscopy was used to assess the absorption capacity of samples for metal ions, and the results of the metal ion adsorption are summarized in Figure 11, where the adsorption efficiency of pure TiO_2 prepared in the absence of organophosphonates was also listed as a reference. Average loading capacities of duplicate tests are reported, and loading capacities for duplicate tests on the same samples varied within 5%. The adsorption efficiency of the Ti-HEDP for Cd^{2+} ions ranged from 23.45% to 26.67%, for the Pb^{2+} ions it ranged from 31.92% to 39.09%, and for the Cu^{2+} ions from 37.62% to 57.55%, which is all higher than that of the pure TiO_2. The selective complexation affinity sequence of metal ions is $Cd^{II} < Pb^{II} < Cu^{II}$. The distribution coefficient (K_d)[10,23] values of 2344–3208 mL/g, 3015–6708 mL/g, and 1531–1818 mL/g were also determined for Ti-HEDP in the adsorption of Pb^{2+}, Cu^{2+}, and Cd^{2+}, respectively. While only 200–400 mL/g was obtained for pure TiO_2. The much higher K_d values of Ti-HEDP than for pure TiO_2 indicate the efficiently increased affinity of the organic–inorganic hybrid sorbent for the metal ion adsorption.

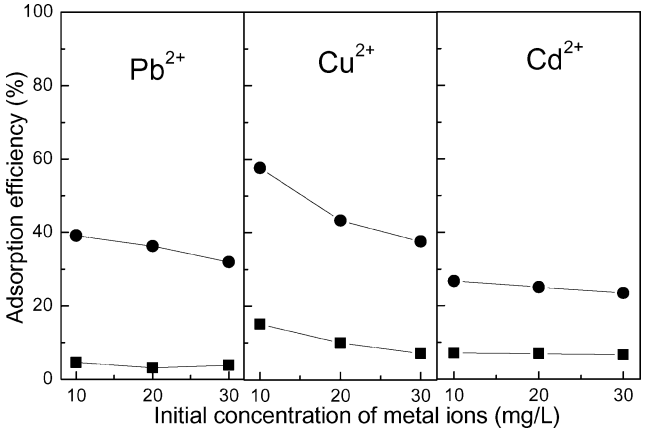

Figure 11. Metal ion adsorption efficiency for Ti-HEDP (−●−) and pure TiO_2 (−■−) materials.

Conclusions

In conclusion, nanostructured titania–phosphonate hybrid materials with a hierarchical macro-/mesoporous structure with a nanorod assembly have been prepared by using 1-hydroxyethane-1,1-diphosphonic acid as organophosphorus coupling molecules. An interesting photocatalytic activity and metal ion adsorption ability were demonstrated for the synthesized materials, suggesting that they have potential in practical applications. The fabrication of other titanium/titania phosphonates with different organic bridging groups and hierarchical nanostructures can also be expected.

Experimental Section

Synthesis: 1-Hydroxyethane-1,1-diphosphonic acid (HEDP, 91 wt.-% aqueous solution, donated by Henan Qingyuan Co.) was used as a coupling molecule for organic moieties of hybrid solids in the synthesis. In a typical synthetic procedure, HEDP (1.03 g) was dissolved in a mixed solution of ethanol (10 mL) and distilled water (30 mL) while stirring, followed by the dropwise addition of tetrabutyl titanate (1.702 g, Kermel, A.R.). After further stirring for 24 h, the mixture was sealed in a Teflon-lined autoclave and heated statically at 80 °C for 24 h. The solid product was collected by filtration, washed with water, and dried overnight at 80 °C in an oven. The sample was characterized as Ti-HEDP. Pure titania was prepared by a similar procedure in the absence of phosphonic acid.

Characterization: Scanning electron microscopy (SEM) and transmission electron microscopy (TEM) were carried out with a Shimadzu SS-550 microscope at 15 keV and a Philips Tecnai G20 at 200 kV, respectively. Fourier transform infrared (FT-IR) spectra were measured with a Bruker VECTOR 22 spectrometer and a KBr-pellet technique. Diffuse reflectance UV/Vis absorption spectroscopy was employed with a JASCO V-570 UV/V/NIR spectrophotometer using $BaSO_4$ as a reference. X-ray diffraction (XRD) patterns were recorded with a Rigaku D/max-2500 diffractometer

with Cu-K_α radiation. Thermogravimetry (TG) and differential scanning calorimetry (DSC) were performed using a Setaram DTA92–16.18 instrument at a heating rate of 5°/min using α-Al_2O_3 as the reference. The chemical compositions of Ti and P were analyzed by inductively coupled plasma (ICP) emission spectroscopy with a Thermo Jarrell-Ash ICP-9000 (N+M) spectrometer, and C, N, and H were analyzed with a Vario-EL elemental analyzer. X-ray photoelectron spectroscopy (XPS) measurements were performed with a Kratos Axis Ultra DLD (delay-line detector) spectrometer equipped with a monochromatic Al-K_α X-ray source (1486.6 eV). Solid-state ^{31}P and ^{13}C magic-angle spinning (MAS) nuclear magnetic resonance (NMR) spectra were recorded with a Varian Infinityplus-400 spectrometer at spinning rates of 12 and 6 kHz and resonance frequencies of 161.9 and 100.5 MHz with recycle times of 5 and 3 s, respectively.

Photocatalytic Activity Testing: The photocatalytic activity experiments were performed by the degradation of Rhodamine B (RhB) dye under either UV or visible-light irradiation in the air at room temperature. In the UV-photocatalytic experiment, the synthesized catalyst (5.5 mg) was placed into a tubular quartz reactor with a RhB aqueous solution (100 mL, 30 mg/L). A 125-W UV lamp with a maximum emission of 365 nm was placed 10 cm higher than the solution surrounded by a circulating water tube. The reaction mixture was stirred under UV-light irradiation. The mixture that was sampled at different times was centrifuged for 5 min to discard any sediment. The absorbance of the reaction solutions was measured with an SP-722 spectrometer at λ_{max} = 554 nm. The visible-light photodecomposition of RhB was carried out with a household desktop lamp with a 40-watt tungsten bulb as the visible-light source, of which the wavelength range is usually 400–2500 nm, and the concentration of the RhB solution and the amount of catalyst used were 1×10^{-5} mol/L and 20 mg, respectively.

Metal Ion Adsorption Testing: Heavy metal ion adsorption tests of the hybrid mesoporous materials were performed in batch mode. The adsorbents (0.01 g) were added to a homoionic solution (50 mL) containing different concentrations (10, 20, 30 mg/L) of $Cu(NO_3)_2$, $Cd(NO_3)_2$, or $Pb(NO_3)_2$. The mixture was stirred for 3 h, followed by centrifugation at 6000 rpm for 15 min. For the Cu^{2+} ion adsorption, the obtained clear solution (20 mL), ethanol (12 mL), and a dicyclohexanoneoxalyldihydrazone solution (30 mL, 0.4 g of dicyclohexanoneoxalyldihydrazone dissolved in 50 mL of ethanol and then adjusted to 500 mL with water) were mixed together and made up to 100 mL with water. The pH was adjusted to between 8 and 9 with ammonia, which is the best pH value for a chromogenic reaction. The volume of Cu^{II} adsorbed was monitored by measuring the UV absorption at λ_{max} = 600 nm of the initial and final solutions. For Cd^{2+} and Pb^{2+} adsorption, 1-(2-pyridinylazo)-2-naphthol and diphenylthiocarbazone were used as chromogenic reagents, respectively, and average loading capacities and efficiencies were also monitored by UV/Vis spectroscopy at λ_{max} (Cd^{2+}) = 555 nm and λ_{max} (Pb^{2+}) = 480 nm. Solubilizing agents (surfactants or emulsifiers) were added for the chromogenic reaction if needed.

Acknowledgments

This work was supported by the National Natural Science Foundation of China (No. 20473041 and 20673060), the National Basic Research Program of China (No. 2003CB615801), the Specialized Research Fund for the Doctoral Program of Higher Education (20070055014), the Chinese–Bulgarian Scientific and Technological Cooperation Project, the MOE Supporting Program for New Century Excellent Talents (NCET-06-0215), and Nankai University.

[1] a) A. Clearfield, Z. Wang, *J. Chem. Soc., Dalton Trans.* **2002**, 2937–2947; b) A. Clearfield, *Curr. Opin. Solid State Mater. Sci.* **2002**, *6*, 495–506.
[2] P. H. Mutin, G. Guerrero, A. Vioux, *J. Mater. Chem.* **2005**, *15*, 3761–3768.
[3] A. Vioux, J. Le Bideau, P. H. Mutin, D. Leclercq, *Top. Curr. Chem.* **2004**, *232*, 145–174.
[4] K. Maeda, *Microporous Mesoporous Mater.* **2004**, *73*, 47–55.
[5] a) T. Kimura, *Chem. Mater.* **2003**, *15*, 3742–3744; b) T. Kimura, *Chem. Mater.* **2005**, *17*, 337–344.
[6] S. Marcinko, A. Y. Fadeev, *Langmuir* **2004**, *20*, 2270–2273.
[7] G. Guerrero, P. H. Mutin, A. Vioux, *Chem. Mater.* **2001**, *13*, 4367–4373.
[8] a) G. Guerrero, P. H. Mutin, A. Vioux, *Chem. Mater.* **2000**, *12*, 1268–1272; b) G. Guerrero, P. H. Mutin, A. Vioux, *J. Mater. Chem.* **2001**, *11*, 3161–3165.
[9] a) J. El. Haskouri, C. Guillem, J. Latorre, A. Beltran, D. Beltran, P. Amoros, *Eur. J. Inorg. Chem.* **2004**, 1804–1807; b) X. Shi, J. Yang, Q. Yang, *Eur. J. Inorg. Chem.* **2006**, 1936–1939.
[10] T. Y. Ma, X. J. Zhang, G. S. Shao, J. L. Cao, Z. Y. Yuan, *J. Phys. Chem. C* **2008**, DOI: 10.1021/jp710636x.
[11] S. Y. Song, J. F. Ma, J. Yang, M. H. Cao, K. C. Li, *Inorg. Chem.* **2005**, *44*, 2140–2142.
[12] S. Y. Song, J. F. Ma, J. Yang, M. H. Cao, H. J. Zhang, H. S. Wang, K. Y. Yang, *Inorg. Chem.* **2006**, *45*, 1201–1207.
[13] M. Vasylyev, E. J. Wachtel, R. Popovitz-Biro, R. Neumann, *Chem. Eur. J.* **2006**, *12*, 3507–3514.
[14] Z. Y. Yuan, T. Z. Ren, B. L. Su, *Adv. Mater.* **2003**, *15*, 1462–1465.
[15] A. Collins, D. Carriazo, S. A. Davis, S. Mann, *Chem. Commun.* **2004**, 568–569.
[16] a) T. Z. Ren, Z. Y. Yuan, A. Azioune, J. J. Pireaux, B. L. Su, *Langmuir* **2006**, *22*, 3886–3894; b) T. Z. Ren, Z. Y. Yuan, B. L. Su, *Chem. Commun.* **2004**, 2730–2731.
[17] M. Kruk, M. Jaroniec, R. Ryoo, S. H. Joo, *Chem. Mater.* **2000**, *12*, 1414–1421.
[18] M. Park, S. Komarneni, *Microporous Mesoporous Mater.* **1998**, *25*, 75–80.
[19] M. Kruk, M. Jaroniec, *Chem. Mater.* **2001**, *13*, 3169–3183.
[20] E. Jaimez, G. B. Hix, R. C. Slade, *Solid State Ionics* **1997**, *97*, 195–201.
[21] E. Jaimez, A. Bortun, G. B. Hix, J. R. Garcia, J. Rodriguez, R. C. T. Slade, *J. Chem. Soc., Dalton Trans.* **1996**, 2285–2292.
[22] T. Z. Ren, Z. Y. Yuan, B. L. Su, *Chem. Phys. Lett.* **2003**, *374*, 170–175.
[23] K. Z. Hossain, L. Mercier, *Adv. Mater.* **2002**, *14*, 1053–1056.

Received: December 27, 2007
Published Online: April 23, 2008

